THE JOURNAL OF PHYSICAL CHEMISTRY Letters

Letter

Cite This: J. Phys. Chem. Lett. 2017, 8, 5537-5542

pubs.acs.org/JPCL

Role of Superexchange Interaction on Tuning of Ni/Li Disordering in Layered $Li(Ni_xMn_yCo_z)O_2$

Jiaxin Zheng,[†,#] Gaofeng Teng,[†,#] Chao Xin,[†,#] Zengqing Zhuo,[†,‡,#] Jiajie Liu,[†] Qinghao Li,[‡,§] Zongxiang Hu,[†] Ming Xu,[†] Shishen Yan,[§] Wanli Yang,[‡] and Feng Pan*[,†]

[†]School of Advanced Materials, Peking University, Shenzhen Graduate School, Shenzhen 518055, People's Republic of China

[‡]Advanced Light Source, Lawrence Berkeley National Laboratory, Berkeley, California 94720, United States

[§]School of Physics, National Key Laboratory of Crystal Materials, Shandong University, Jinan 250100, People's Republic of China

Supporting Information

ABSTRACT: Ni/Li exchange (disordering) usually happens in layered $Li(Ni_xMn_yCo_z)O_2$ (NMC) materials and affects the performance of the material in lithium-ion batteries. Most of previous studies attributed this phenomenon to the similar size of Ni^{2+} and Li^+, which implies that Ni^{2+} should be more favorable than Ni^{3+} to be located at Li 3b sites in the Li slab. However, this theory cannot explain why in Ni-rich NMC materials where most Ni cations are Ni^{3+}, Ni/Li exchange happens even more frequently. Using extensive ab initio calculations combined with experiments, here we report that a superexchange interaction between transition metals plays a dominating role in tuning the Ni/Li disordering in NMC materials. Under this scheme, we also propose a new charge compensation mechanism that describes that after Ni^{3+}/Li exchange the nearest Co^{3+} transforms to Co^{4+} in Ni-rich NMC materials. On the basis of this theory, the existence of Co^{4+} in the initial Ni-rich NMC samples was predicted for the first time, which was further confirmed by our synchrotron-based soft X-ray absorption spectroscopy.

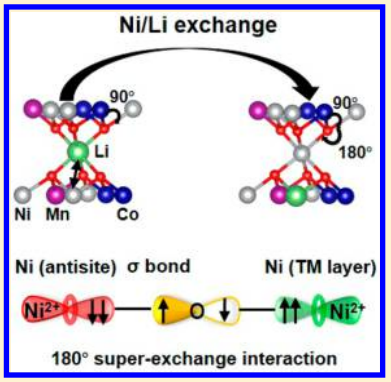

Rechargeable lithium-ion batteries (LIBs) play an important role in our lives to power most of today's portable electronics and electrical vehicles (EVs).[1,2] Owing to the higher energy density, higher reversible capacity, lower cost, and better environmental compatibility than the traditional $LiCoO_2$, layered $Li(Ni_xMn_yCo_z)O_2$ (NMC, $x + y + z = 1$) materials from solid-solution approaches to $LiMO_2$ (M = Ni, Mn, Co, etc.) have been extensively studied as important cathode materials for high-energy-density and EV LIBs.[3] The NMC materials consist of alternative layers of Li ions and transition-metal (TM) ions separated by oxygen atomic layers. Ni/Li exchange (or Ni/Li disordering) usually happens between the Li layer and TM layer in these materials during synthesis and electrochemical cycling.[3−13] Such Ni/Li exchange would affect the performance of NMC materials in different ways, as summarized by the following: (i) The antisite Ni ions in the Li layer will reduce the Li-ion layer space and consequently decrease the Li-ion diffusion coefficients (a small decrease of ~0.02 Å for Li layer space resulting in an increase of the activation barrier by 20 to 30 meV).[14,15] (ii) The antisite Ni ions in the Li-ion layer gradually migrate to the particle surface, leading to Ni depletion in the bulk, structural instability, and consequently cathode voltage and capacity fade.[16,17] (iii) The Ni/Li exchange leads to obvious anisotropic stress[15] and affects the structural stability of NMC materials.[18] (iv) Different from the above three disadvantages, a few studies showed that some degree of disorder can mitigate the slab-distance contraction at high states of charge, thus benefiting the structural stability during electrochemical cycling.[19,20] Thus understanding and then tuning the Ni/Li disordering becomes important to improve the performance of NMC materials.

In general, the Li/Ni disordering in NMC materials can be controlled by carefully tuning the temperature and holding time in synthesis and heating. However, this approach requires lengthy synthesis process and cannot prevent the occurrence of Ni/Li disordering during electrochemical cycling. Previous experiments also found that when using the same synthesis approach the degree of Ni/Li disordering in NMC materials varies with the Ni, Co, and Mn contents.[12,17] For example, the $Li(Ni_{0.6}Mn_{0.3}Co_{0.1})O_2$ has an obvious higher Li−Ni disorder level (6.9(6)%) than $Li(Ni_{0.4}Mn_{0.4}Co_{0.2})O_2$ (2.7(3)%) under the same synthesis temperature.[12] Calcined at the same temperature of 850 °C, $Li(Ni_{0.33}Mn_{0.33}Co_{0.33})O_2$ showed the lowest content (1.56%) of Ni/Li disordering, $Li(Ni_{0.4}Mn_{0.4}Co_{0.2})O_2$ showed moderate content, and $Li(Ni_{0.5}Mn_{0.3}Co_{0.2})O_2$ showed the highest content (3.34%).[21] Using a scanning transmission electron microscopy (STEM) technique, we previously found that the contents of Ni/Li exchange in $Li(Ni_{0.4}Mn_{0.4}Co_{0.2})O_2$, $Li(Ni_{0.5}Mn_{0.5})O_2$, and $Li(Ni_{0.6}Mn_{0.2}Co_{0.2})O_2$ were 12.4, 14.5, and 15%,[17] respectively. A previous experimental study also found that the content of Ni/Li exchange in $LiNi_yMn_yCo_{1-2y}O_2$ can be reduced by increasing the Co content.[22] Hereto, a question is raised: What

Received: September 21, 2017
Accepted: October 31, 2017
Published: October 31, 2017

DOI: 10.1021/acs.jpclett.7b02498
J. Phys. Chem. Lett. 2017, 8, 5537−5542

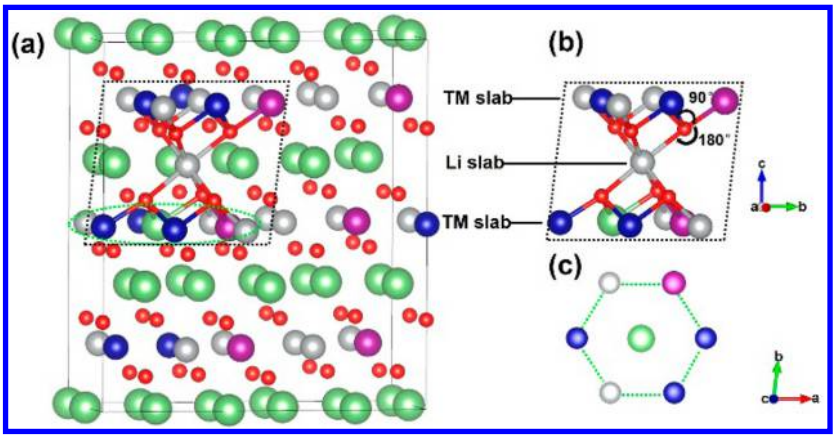

Figure 1. (a) Structure model for the multilattice of $Li(Ni_{0.6}Mn_{0.2}Co_{0.2})O_2$ (622) with one pair of Ni/Li exchange. (b) $(TM)_6$−O_3−Ni−O_3−$Li(TM)_5$ coordination structure unit for the antisite Ni in Li slab. (c) Ion environment of the antisite Li in the transition-metal layer. Green: Li; red: O; silver: Ni; purple: Mn; blue: Co.

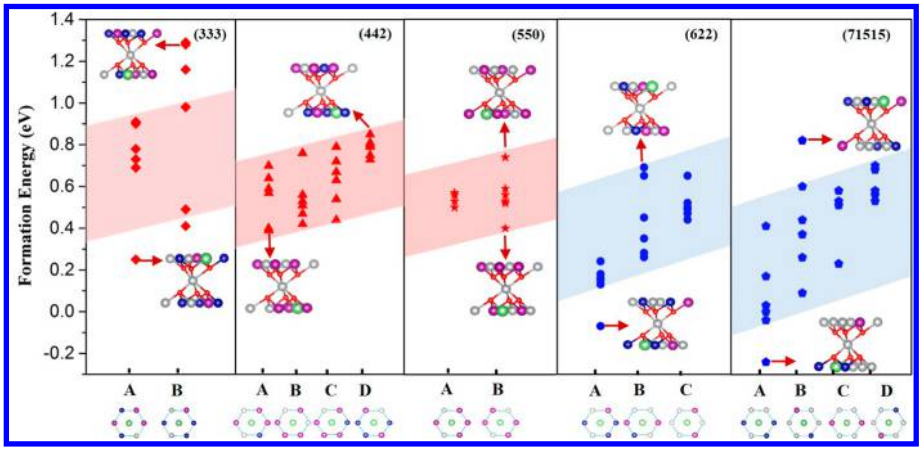

Figure 2. Formation energy (E^f) of one pair of Ni/Li exchange in (333), (442), (550), (622), and (71515) with zigzag TM arrangements. The local configurations of Ni/Li exchanges with the lowest and highest E^f are shown in each material. The shaded areas show the general trend of the E^f variation for the Ni/Li exchange, and the schematics at the bottom represent the nonequivalent ion environment for the antisite Li ion in the TM layer.

is the role of transition metals in affecting the Ni/Li disordering in the layered NMC materials? Using ab initio calculations, here we investigate the characteristic of Ni/Li disordering in NMC materials. Interestingly, it was found that a superexchange interaction between transition metals plays a critical role in tuning the Ni/Li disordering.

The studied NMC materials include $Li(Ni_{0.33}Mn_{0.33}Co_{0.33})O_2$ (333), $Li(Ni_{0.4}Mn_{0.4}Co_{0.2})O_2$ (442), $Li(Ni_{0.5}Mn_{0.5})O_2$ (550), $Li(Ni_{0.6}Mn_{0.2}Co_{0.2})O_2$ (622), and $Li(Ni_{0.7}Mn_{0.15}Co_{0.15})O_2$ (71515). According to the classification in our previous works,[18,23] (333), (442), and (550) are three representative NMC materials of "Ni = Mn" group with pure Ni^{2+} state; (622) and (71515) are two representative materials of "Ni-rich" group NMC materials with mixed valence states of Ni^{2+}/Ni^{3+}. (442) and (622) contain the same content of Co, and (333), (442) and (550) are in the same group but contain different contents of Co. The zigzag arrangement of TM ions in the TM layer was adopted for the structure models of the five NMC materials (Figure S1). Figure 1a shows the supercell of (622) with a zigzag arrangement of TM ions and one pair of Ni/Li exchange. Each antisite Ni in Li layer connects to six nearest TMs in the upside TM layer and five nearest TMs and one Li ion in the downside TM layer through the intermediate six oxygen atoms and forms a $(TM)_6$−O_3−Ni−O_3−$Li(TM)_5$ coordination structure unit (Figure 1b). The antisite Li in the TM layer is surrounded by the six nearest TM ions (Figure 1c). The supercell of (550) with the flower arrangement of TM ions and one pair of Ni/Li exchange was also considered (Figure S2). The calculated crystal parameters of the NMC materials are very close to the experimental data (Table S2).[12,24−26] According to the nonequivalent Ni sites in the TM layer (or the nonequivalent antisite Li in TM layer) (Figure S1), we divided all of the Ni/Li exchange pairs into two groups (A and B) in (333), four groups (A−D) in (442), two groups (A and B) in (550), three groups (A−C) in (622), and four groups (A−D) in (71515), as shown in Figure S4.

Figure 2 shows a comparison of the calculated formation energies of one pair of Ni/Li exchange in the five NMC materials with zigzag arrangements for TM ions (detailed values are shown in Figure S5). From the overall view in Figure 2, we can see that with the same cobalt content the E^f values of Ni/Li exchange pairs in (622) are generally much smaller than those in (442), indicating that the Ni/Li exchange is more likely to happen in Ni-rich NMC materials, and this finding is consistent with the experimental observations.[12,17] Although (550), (442), and (333) are NMC materials in the same "Ni═Mn" group, the E^f values generally increase in the order of: (550) (especially with flower structure) < (442) < (333), which

DOI: 10.1021/acs.jpclett.7b02498
J. Phys. Chem. Lett. 2017, 8, 5537−5542

means that Ni/Li exchange is more likely to happen in "Ni═Mn" NMC materials with less Co content, as supported by the previous experimental results.[5,9,14,27] Interestingly, for each group of Ni/Li exchange pairs in the five NMC materials (Figures S6 and S7), it can be found that more Ni^{2+}−O−Ni^{2+} linear structures in $(TM)_6$−O_3−Ni−O_3−$(TM)_5$ units would generally lead to smaller E^f. Moreover, in "Ni═Mn" NMC materials, the Ni ion with more nearest Co ions in the TM layer would be the hardest to exchange with Li (Figure 2 and Figure S5), whereas in "Ni-rich" NMC materials the Ni ion with more nearest Co ions in the TM layer would be the easiest to exchange with Li (Figure 2 and Figure S5). A more detailed discussion about the above calculated formation energies of Ni/Li exchange can be found in Section S2 in the Supporting Information (SI).

To explain the above findings, electronic structures of the representative (442), (550), and (622) without and with Ni/Li exchange were further analyzed. It can be seen that in "Ni = Mn" NMC materials with pure Ni^{2+} state, the antisite Ni ions show the same Ni^{2+} state but with a spin-flip, and the Co^{3+} and Mn^{4+} remain unchanged after Ni^{2+}/Li exchange (see detailed discussion in Section S3 in the SI). The Co ions and Mn ions in (622) without Ni/Li exchange show the same electronic configurations (Co^{3+}: $t_{2g}^6e_g^0$ (−0.03 μ_B); Mn^{4+}: $t_{2g}^3e_g^0$ (−3.16 μ_B)) as in (442) and (550) (Figure 3a and Table S3), whereas for

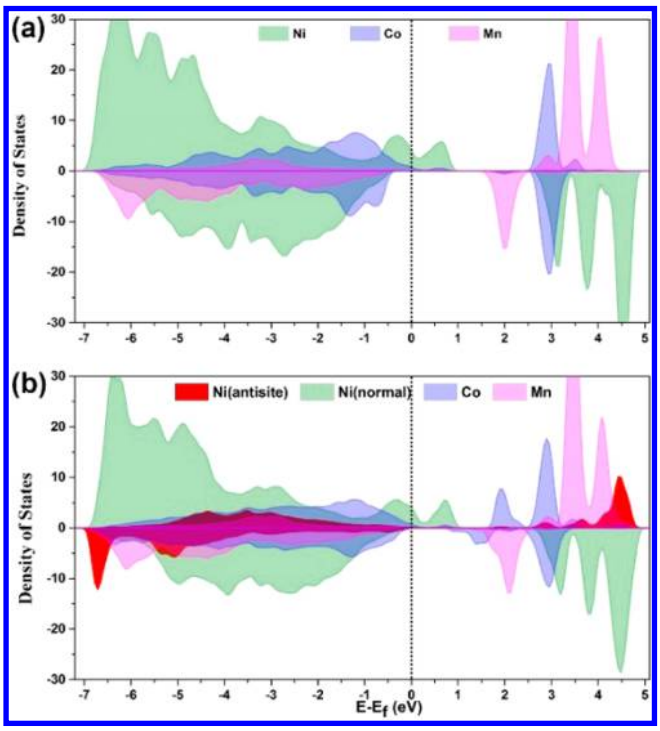

Figure 3. Projected density of states (PDOS) of the transition metal ions for (622) without (a) and with (b) Ni/Li exchange. The PDOS represents the projection on the sum of all equivalent TMs in the unit cell.

"Ni-rich" NMC materials, Ni ions show mixed valence states of Ni^{2+}/Ni^{3+} (with magnetic moments of 1.72 μ_B/1.28 μ_B in (622)). In Figure 3a, the peak just above the Fermi level shows the spin-up e_g orbitals of Ni^{3+}. Interestingly, in group A Ni/Li exchanges with the smallest E^f, and the antisite Ni ions are all in the 3+ valence state (2+ valence state for the B and C groups) in the TM layer before exchanging with Li. Then, they change to the valence state of Ni^{2+} in the Li layer with the magnetic moment opposite to the Ni ions in the TM layer (in red) (Figure 3b). More importantly, the nearest Co changes its valence state from Co^{3+} (−0.03 μ_B) to Co^{4+} (−1.14 μ_B) to make charge compensation at the same time (Table S3), which can also be observed from the new unoccupied states above the Fermi level for the PDOS of Co (Figure 3b). More discussions about this charge compensation can be found in Section S4 in the SI. No matter without or with Ni/Li exchange, Mn ions always show an unchanged state of Mn^{4+}. (71515) shows the similar electronic structure as (622) (Figure S14). Thus in "Ni-rich" NMC materials with mixed valence states of Ni^{2+}/Ni^{3+}, Ni^{3+} has the priority to exchange with Li and changes to a Ni^{2+} state with a spin-flip and the addition of an electron from the nearest Co (Co^{3+}), and the nearest Co changes from Co^{3+} to Co^{4+} due to the charge compensation after Ni^{3+}/Li exchange.

In the TM layer, due to the unpaired electrons in d orbitals, Ni^{2+}/Ni^{3+} forms 90° intralayer superexchanges with neighboring TM cations via bridged O anion. When Li/Ni exchange happens, the antisite Ni^{2+} with the magnetic moment opposite to the Ni ions in the TM layer easily forms 180° (linear) superexchanges with Ni^{2+}, Ni^{3+}, and Mn^{4+} in the TM layer via the σ bond formed between the e_g orbital of the antisite Ni^{2+} and the p orbital of O^{2-} (Figure 4a,b). Because of the stronger σ bond, the 180° magnetic interactions are always stronger than the 90° interactions.[28−30] Different from direct interaction, superexchange interaction needs the O ion as a carrier. The p orbitals of intervening oxygen whose axis points to the cations participate in the superexchange interaction via the σ bond formed between the d orbital of TM cations and the p orbital of O^{2-}: An electron is first transferred from the pσ-orbital to one of the neighboring TM cation, and the unpaired spin left on O^{2-} couples to the spin of the other neighboring TM cation through exchange interaction.[28] So, the spin density of the O ion can reflect the strength of superexchange interactions. Thus the strengths of different kinds of 180° superexchange interactions can be analyzed by 3D spin electron density maps. From Figure 4c−g, it can be seen that among the linear superexchanges, the spin density of O^{2-} in the linear antiferromagnetic (AF) Ni^{2+}−O^{2-}−Ni^{2+} is the largest (Figure 4c), indicating the strongest superexchange interaction. This can be attributed to the fact that Ni^{2+} has two unpaired electrons, and the superexchange in Ni^{2+}−O^{2-}−Ni^{2+} (e_g−2p−e_g) takes effect through the same e_g orbital with perfect energy alignment. The linear ferromagnetic (FM) Ni^{2+}−O^{2-}−Mn^{4+} (e_g−2p−t_{2g}) and FM Ni^{2+}−O^{2-}−Co^{4+} (e_g−2p−t_{2g}) superexchanges are weaker (Figure 4e,f), and the linear AF Ni^{2+}−O^{2-}−Ni^{3+} (e_g−2p−e_g) superexchange is moderate (Figure 4d). This trend is consistent with previous magnetic properties measurements in layered $LiNi_yMn_yCo_{1-2y}O_2$.[30] Because of the absence of unpaired electron in the electronic configuration of Co^{3+}, the Ni^{2+}−O^{2-}−Co^{3+} superexchange is the weakest (Figure 4g). The comparison among the energetics of different magnetic configurations further confirms the existence of the above superexchange interactions (Section S5 in the SI).

Now the Ni/Li exchange properties in NMC materials can be understood. Because of the very strong linear AF Ni^{2+}−O^{2-}−Ni^{2+} superexchange, the antisite $(TM)_6$−O_3−Ni−O_3−$(TM)_5$ units with more Ni^{2+}−O^{2-}−Ni^{2+} linear structures show the smaller E^f of Ni/Li exchange in all NMC materials. Because the Ni^{2+}−O^{2-}−Co^{3+} superexchange is very weak, Co^{3+} can suppress the Ni/Li exchange. This explains why in "Ni═Mn" NMC materials the Ni ion with more nearest Co ions in the

DOI: 10.1021/acs.jpclett.7b02498
J. Phys. Chem. Lett. 2017, 8, 5537−5542

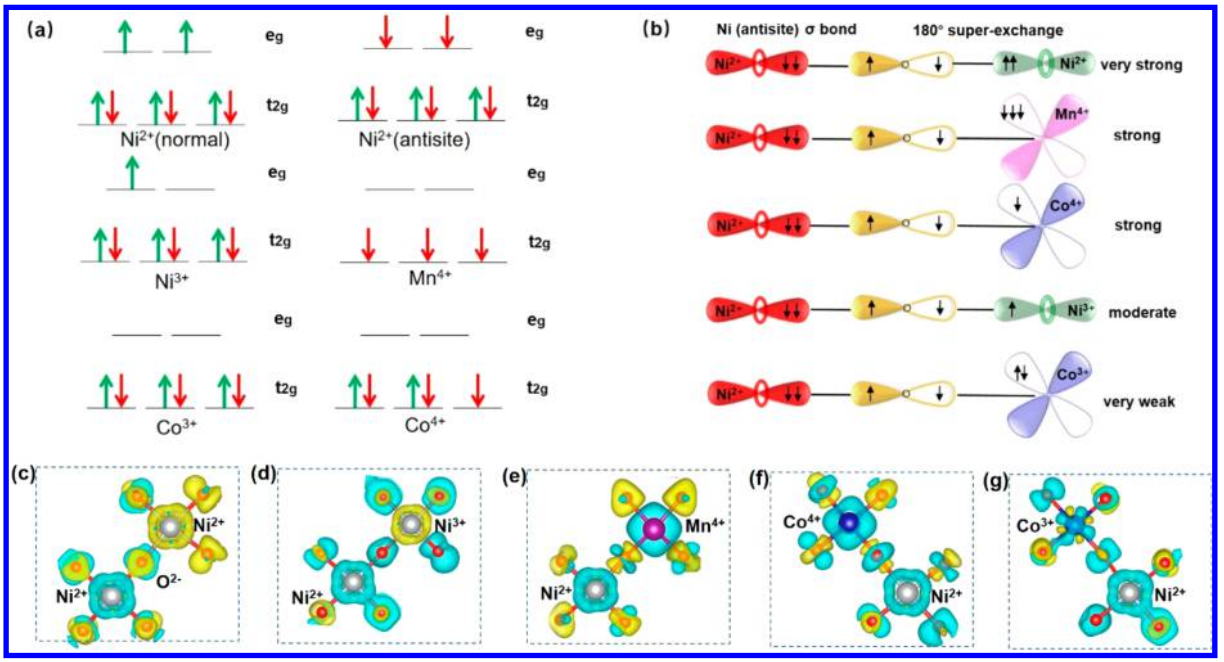

Figure 4. (a) Electronic configurations for TM ion in NMC materials. (b) Schematic for 180° superexchange interaction. (c–g) 3D spin electron density maps of different kinds of 180° superexchange interactions. Blue and yellow denote spin up and spin down, respectively. The isovalues for the isosurfaces of the spin densities were 0.05 e $Å^{-3}$ for all cases.

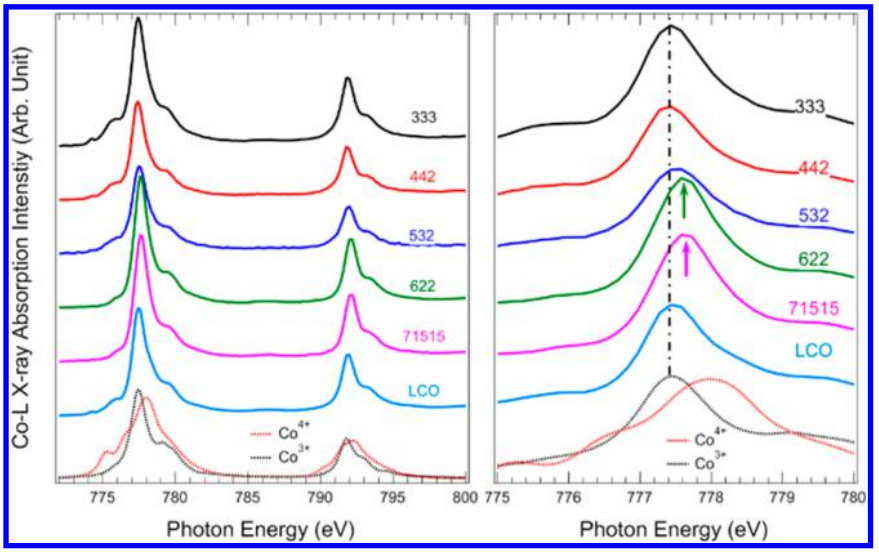

Figure 5. Co *L*-edge sXAS spectra collected on a series of NMC samples in comparison with a standard $LiCoO_2$ (LCO) and reference $Co^{3+/4+}$ spectra. The right panel shows the enlarged Co-L_3 edge. Arrows indicate the main peak position shifts of (622) and (71515) systems, which emphasizes the shift toward higher energy.

TM layer is the hardest to exchange with Li. In "Ni-rich" NMC materials with mixed states of Ni^{2+}/Ni^{3+}, the Ni surrounded by three nearest Co in the TM layer shows the valence state of Ni^{3+}. Compared with Ni^{2+} in the TM layer, it has the priority to exchange with Li and transforms to a Ni^{2+} state with a spin-flip to form more linear AF $Ni^{2+}–O^{2-}–Ni^{2+}$ superexchanges because the linear AF $Ni^{2+}–O^{2-}–Ni^{3+}$ exchange is much weaker. Moreover, as the nearest Co^{3+} in the TM layer changes to Co^{4+} with an unpaired electron in the t_{2g} orbitals after Ni^{3+}/Li exchange, a new interlayer linear FM $Ni^{2+}–O^{2-}–Co^{4+}$ superexchange and new 90° intralayer AF $Co^{4+}–O^{2-}–Ni^{2+}/Ni^{3+}$ superexchanges would be formed to further lower the structure energy, as indicated from the large overlapping between the Ni-e_g orbitals and Co-t_{2g} orbitals (Figure 3b). This explains why the Ni ion with more nearest Co ions in the TM layer is the easiest to exchange with Li in "Ni-rich" NMC materials.

Finally, under our superexchange model, we predict the charge compensation that after Ni^{3+}/Li exchange the nearest Co^{3+} transforms to Co^{4+} in "Ni-rich" NMC materials. Under this prediction, for the initial NMC samples (without any delithiation) with some content of Ni/Li exchange, Co^{4+} should be detected in "Ni-rich" NMC materials, and only Co^{3+} can be detected in "Ni═Mn" NMC materials. To verify this, we synthesized $LiCoO_2$, (333), (442), (532), (622), and (71515) (see details in the SI) and measured the oxidation states of Co in the samples through sXAS, as shown in Figure 5. sXAS has been demonstrated as a direct probe of the 3d states

DOI: 10.1021/acs.jpclett.7b02498
J. Phys. Chem. Lett. 2017, 8, 5537–5542

of transition-metal elements through its dipole-allowed 2p−3d transitions.[31] In particular, the main peak shift of the Co-L_3 edge could be used to define the Co valence quasi-quantitatively.[31] For a direct comparison, we plotted two reference spectra collected on $LiCoO_2$ (Co^{3+}) and fully delithiated Li_0CoO_2 (Co^{4+}). Our reference results are consistent with previous publications,[32−35] which clearly shows that the main peak of Co-L edge sXAS shifts toward higher energy when the formal valence increases. Figure 5 shows that the main peaks of NMC (622) and (71515) are obviously higher in energy than that of $LiCoO_2$, NMC (333), (442), and Co^{3+} reference. The peak of NMC (532) sits in the middle. Although the main peak position of the (532), (622), and (71515) does not reach the energy of Co^{4+}, the obvious increase in peak energy indicates that the Co valence in these systems is partially oxidized to Co^{4+}. A quasi-quantitative analysis based on the Co-L main peak position could be used to estimate the Co^{4+} concentration.[31] The energy loss between $LiCoO_2$/Co^{3+} and 532 is 0.05 eV, indicating that there is ∼10% Co^{4+} in 532 sample. Similarly, the difference between $LiCoO_2$ and (622)/(71515) is almost 0.1 eV, so there is ∼20% Co^{4+} (622)/(71515). Therefore, these experimental results on Co oxidation states directly confirm our theoretical conclusions and the superexchange interaction model.

In summary, the superexchange interactions between transition metals play a critical role in tuning the Ni/Li disordering by affecting the E^f of Ni/Li exchange in NMC materials (the discussion about the driving force for the Ni/Li exchange can be seen in Section S7 in the SI). In all NMC materials, with a "spin-flip" for the antisite Ni^{2+}, Ni/Li exchange most likely happens at the place to form more strong linear AF Ni^{2+}−O^{2-}−Ni^{2+} superexchanges. Thus the Ni/Li exchange is most likely to happen in NMC materials with a higher Ni content (especially a higher Ni^{2+} content). Because of the weak Ni^{2+}−O^{2-}−Co^{3+} superexchange, Co doping can suppress the Ni/Li exchange in "Ni═Mn" NMC materials, whereas in NMC materials with mixed valence states of Ni^{2+}/Ni^{3+}, Ni^{3+} has the priority to exchange with Li and changes to a Ni^{2+} state with a spin flip, to form more strong linear AF Ni^{2+}−O^{2-}−Ni^{2+} superexchanges. What is more, due to the charge compensation after Ni^{3+}/Li exchange, the nearest Co^{3+} transforms to Co^{4+}, thus forming new linear interlayer FM Ni^{2+}−O^{2-}−Co^{4+} and 90° intralayer AF Co^{4+}−O^{2-}−Ni^{2+}/Ni^{3+} superexchanges. This would further promote the Ni/Li exchange. This new charge compensation mechanism was also confirmed by our synchrotron-based soft X-ray absorption spectroscopy. These findings would share important clues on how to control the Ni/Li exchange degrees in NMC materials. For example, to obtain NMC materials with low content of Ni/Li exchange, we can reduce the Ni^{2+} content (by reducing the Mn^{4+} content) and increase the Co content during synthesis or find other transition metals that could play the same role as Co (see discussion in Section S8 in the SI).

■ ASSOCIATED CONTENT

Supporting Information

The Supporting Information is available free of charge on the ACS Publications website at DOI: 10.1021/acs.jpclett.7b02498.

Ab initio calculation and experimental methods, more details and discussions about the calculated results, discussion about the charge compensation of Co^{3+} to Co^{4+} after the Li/Ni exchange with Ni^{3+} transforming to Ni^{2+} in (622), and Co L-edge sXAS spectra (TFY) collected on a serious of initial NMC samples without any delithiation. (PDF)

■ AUTHOR INFORMATION

Corresponding Author

*E-mail: panfeng@pkusz.edu.cn.

ORCID

Wanli Yang: 0000-0003-0666-8063

Feng Pan: 0000-0002-8216-1339

Author Contributions

#J.Z., G.T., C.X., and Z.Z. contributed equally to this work.

Notes

The authors declare no competing financial interest.

■ ACKNOWLEDGMENTS

This work was financially supported by National Materials Genome Project (2016YFB0700600), the National Natural Science Foundation of China (Nos. 21603007 and 51672012), and Shenzhen Science and Technology Research Grant (Nos. JCYJ20150729111733470 and JCYJ20151015162256516). sXAS data were collected at beamline 8.0.1 of the Advanced Light Source, which is supported by the Director, Office of Science, Office of Basic Energy Sciences, of the U.S. Department of Energy under Contract No. DE-AC02-05CH11231. We also thank Dr. Haibiao Chen for the English language improvement.

■ REFERENCES

(1) Armand, M.; Tarascon, J. M. Building Better Batteries. *Nature* **2008**, *451*, 652−657.

(2) Goodenough, J. B.; Park, K. S. The Li-Ion Rechargeable Battery: A Perspective. *J. Am. Chem. Soc.* **2013**, *135*, 1167−1176.

(3) Goodenough, J. B.; Kim, Y. Challenges for Rechargeable Li Batteries. *Chem. Mater.* **2010**, *22*, 587−603.

(4) Breger, J.; Meng, Y. S.; Hinuma, Y.; Kumar, S.; Kang, K.; Shao-Horn, Y.; Ceder, G.; Grey, C. P. Effect of High Voltage on the Structure and Electrochemistry of $LiNi_{0.5}Mn_{0.5}O_2$: A Joint Experimental and Theoretical Study. *Chem. Mater.* **2006**, *18*, 4768−4781.

(5) Hinuma, Y.; Meng, Y. S.; Kang, K. S.; Ceder, G. Phase Transitions in the $LiNi_{0.5}Mn_{0.5}O_2$ System with Temperature. *Chem. Mater.* **2007**, *19*, 1790−1800.

(6) Hoang, K.; Johannes, M. Defect Physics and Chemistry in Layered Mixed Transition Metal Oxide Cathode Materials: (Ni, Co, Mn) Vs (Ni, Co, Ai). *Chem. Mater.* **2016**, *28*, 1325−1334.

(7) Li, H. H.; Yabuuchi, N.; Meng, Y. S.; Kumar, S.; Breger, J.; Grey, C. P.; Shao-Horn, Y. Changes in the Cation Ordering of Layered O3 $Li_xNi_{0.5}Mn_{0.5}O_2$ During Electrochemical Cycling to High Voltages: An Electron Diffraction Study. *Chem. Mater.* **2007**, *19*, 2551−2565.

(8) Whittingham, M. S. Lithium Batteries and Cathode Materials. *Chem. Rev.* **2004**, *104*, 4271−4301.

(9) Lian, F.; Axmann, P.; Stinner, C.; Liu, Q. G.; Wohlfahrt-Mehrens, M. Comparative Study of the Preparation and Electrochemical Performance of $LiNi_{1/2}Mn_{1/2}O_2$ Electrode Material for Rechargeable Lithium Batteries. *J. Appl. Electrochem.* **2008**, *38*, 613−617.

(10) Yabuuchi, N.; Kumar, S.; Li, H. H.; Kim, Y. T.; Shao-Horn, Y. Changes in the Crystal Structure and Electrochemical Properties of $Li_xNi_{0.5}Mn_{0.5}O_2$ During Electrochemical Cycling to High Voltages. *J. Electrochem. Soc.* **2007**, *154*, A566−A578.

(11) Chen, H.; Dawson, J. A.; Harding, J. H. Effects of Cationic Substitution on Structural Defects in Layered Cathode Materials $Linio_2$. *J. Mater. Chem. A* **2014**, *2*, 7988−7996.

(12) Ngala, J. K.; Chernova, N. A.; Matienzo, L.; Zavalij, P. Y.; Whittingham, M. S. The Syntheses and Characterization of Layered

DOI: 10.1021/acs.jpclett.7b02498
J. Phys. Chem. Lett. 2017, 8, 5537−5542

$LiNi_{1-y-z}Mn_yCo_zO_2$ Compounds. *Mater. Res. Soc. Symp. Proc.* **2003**, *756*, 231−236.
(13) Park, M. S. First-Principles Study of Native Point Defects in $LiNi_{1/3}Co_{1/3}Mn_{1/3}O_2$ and Li_2MnO_3. *Phys. Chem. Chem. Phys.* **2014**, *16*, 16798−16804.
(14) Kang, K. S.; Meng, Y. S.; Breger, J.; Grey, C. P.; Ceder, G. Electrodes with High Power and High Capacity for Rechargeable Lithium Batteries. *Science* **2006**, *311*, 977−980.
(15) Yu, H. J.; Qian, Y. M.; Otani, M. R.; Tang, D. M.; Guo, S. H.; Zhu, Y. B.; Zhou, H. S. Study of the Lithium/Nickel Ions Exchange in the Layered $LiNi_{0.42}Mn_{0.42}Co_{0.16}O_2$ Cathode Material for Lithium Ion Batteries: Experimental and First-Principles Calculations. *Energy Environ. Sci.* **2014**, *7*, 1068−1078.
(16) Yan, P. F.; Nie, A. M.; Zheng, J. M.; Zhou, Y. G.; Lu, D. P.; Zhang, X. F.; Xu, R.; Belharouak, I.; Zu, X. T.; Xiao, J.; et al. Evolution of Lattice Structure and Chemical Composition of the Surface Reconstruction Layer in $Li_{1.2}Ni_{0.2}Mn_{0.6}O_2$ Cathode Material for Lithium Ion Batteries. *Nano Lett.* **2015**, *15*, 514−522.
(17) Yan, P. F.; Zheng, J. M.; Lv, D. P.; Wei, Y.; Zheng, J. X.; Wang, Z. G.; Kuppan, S.; Yu, J. G.; Luo, L. L.; Edwards, D.; et al. Atomic-Resolution Visualization of Distinctive Chemical Mixing Behavior of Ni, Co, and Mn with Li in Layered Lithium Transition-Metal Oxide Cathode Materials. *Chem. Mater.* **2015**, *27*, 5393−5401.
(18) Zheng, J. X.; Liu, T. C.; Hu, Z. X.; Wei, Y.; Song, X. H.; Ren, Y.; Wang, W. D.; Rao, M. M.; Lin, Y.; Chen, Z. H.; et al. Tuning of Thermal Stability in Layered $Li(Ni_xMn_yCo_z)O_2$. *J. Am. Chem. Soc.* **2016**, *138*, 13326−13334.
(19) Urban, A.; Lee, J.; Ceder, G. The Configurational Space of Rocksalt-Type Oxides for High-Capacity Lithium Battery Electrodes. *Adv. Energy Mater.* **2014**, *4*, 1400478.
(20) Meng, Y. S.; Ceder, G.; Grey, C. P.; Yoon, W. S.; Jiang, M.; Breger, J.; Shao-Horn, Y. Cation Ordering in Layered O3 $Li[Ni_xLi_{1/3-2x/3}]Mn_{2/3-X/3}]O_2$ ($0 \le X \le 1/2$). *Chem. Mater.* **2005**, *17*, 2386−2394.
(21) Julien, C.; Mauger, A.; Zaghib, K.; Groult, H. Optimization of Layered Cathode Materials for Lithium-Ion Batteries. *Materials* **2016**, *9*, 595.
(22) Ngala, J. K.; Chernova, N. A.; Ma, M.; Mamak, M.; Zavalij, P. Y.; Whittingham, M. S. The Synthesis, Characterization and Electrochemical Behavior of the Layered $LiNi_{0.4}Mn_{0.4}Co_{0.2}O_2$ Compound. *J. Mater. Chem.* **2004**, *14*, 214−220.
(23) Wei, Y.; Zheng, J. X.; Cui, S. H.; Song, X. H.; Su, Y. T.; Deng, W. J.; Wu, Z. Z.; Wang, X. W.; Wang, W. D.; Rao, M. M.; et al. Kinetics Tuning of Li-Ion Diffusion in Layered $Li(Ni_xMn_yCo_z)O_2$. *J. Am. Chem. Soc.* **2015**, *137*, 8364−8367.
(24) Piskin, B.; Aydinol, M. K. Development and Characterization of Layered $Li(Ni_xMn_yCo_{1-X-Y})O_2$ Cathode Materials for Lithium Ion Batteries. *Int. J. Hydrogen Energy* **2016**, *41*, 9852−9859.
(25) Yue, P.; Wang, Z. X.; Peng, W. J.; Li, L. J.; Guo, H. J.; Li, X. H.; Hu, Q. Y.; Zhang, Y. H. Preparation and Electrochemical Properties of Submicron $LiNi_{0.6}Co_{0.2}Mn_{0.2}O_2$ as Cathode Material for Lithium Ion Batteries. *Scr. Mater.* **2011**, *65*, 1077−1080.
(26) Cao, H.; Zhang, Y.; Zhang, H.; Xia, B. J. Synthesis and Electrochemical Characteristics of Layered $LiNi_{0.6}Co_{0.2}Mn_{0.2}O_2$ Cathode Material for Lithium Ion Batteries. *Solid State Ionics* **2005**, *176*, 1207−1211.
(27) Ellis, B. L.; Lee, K. T.; Nazar, L. F. Positive Electrode Materials for Li-Ion and Li-Batteries. *Chem. Mater.* **2010**, *22*, 691−714.
(28) Kanamori, J. Superexchange Interaction and Symmetry Properties of Electron Orbitals. *J. Phys. Chem. Solids* **1959**, *10*, 87−98.
(29) Goodenough, J. B. *Magnetism and the Chemical Bond*; Interscience: New York, 1963.
(30) Chernova, N. A.; Ma, M.; Xiao, J.; Whittingham, M. S.; Breger, J.; Grey, C. P. Layered $Li_xNi_yMn_yCo_{1-2y}O_2$ Cathodes for Lithium Ion Batteries: Understanding Local Structure Via Magnetic Properties. *Chem. Mater.* **2007**, *19*, 4682−4693.
(31) Li, Q.; Qiao, R.; Wray, L. A.; Chen, J.; Zhuo, Z.; Chen, Y.; Yan, S.; Pan, F.; Hussain, Z.; Yang, W. Quantitative Probe of the Transition Metal Redox in Battery Electrodes through Soft X-Ray Absorption Spectroscopy. *J. Phys. D: Appl. Phys.* **2016**, *49*, 413003.
(32) Cherkashinin, G.; Motzko, M.; Schulz, N.; Späth, T.; Jaegermann, W. Electron Spectroscopy Study of Li[Ni, Co, Mn]O_2/Electrolyte Interface: Electronic Structure, Interface Composition, and Device Implications. *Chem. Mater.* **2015**, *27*, 2875−2887.
(33) Chen, J.-M.; Chin, Y.-Y.; Valldor, M.; Hu, Z.; Lee, J.-M.; Haw, S.-C.; Hiraoka, N.; Ishii, H.; Pao, C.-W.; Tsuei, K.-D.; et al. A Complete High-to-Low Spin State Transition of Trivalent Cobalt Ion in Octahedral Symmetry in $SrCo_{0.5}Ru_{0.5}O_{3-\delta}$. *J. Am. Chem. Soc.* **2014**, *136*, 1514−1519.
(34) Cherkashinin, G.; Jaegermann, W. Dissociative Adsorption of H_2O on $LiCoO_2$ (00 L) Surfaces: Co Reduction Induced by Electron Transfer from Intrinsic Defects. *J. Chem. Phys.* **2016**, *144*, 184706.
(35) Ikeno, H.; Mizoguchi, T.; Koyama, Y.; Ogumi, Z.; Uchimoto, Y.; Tanaka, I. Theoretical Fingerprints of Transition Metal L2,3 XANES and ELNES for Lithium Transition Metal Oxides by Ab Initio Multiplet Calculations. *J. Phys. Chem. C* **2011**, *115*, 11871−11879.

DOI: 10.1021/acs.jpclett.7b02498
J. Phys. Chem. Lett. 2017, 8, 5537−5542